Nonlinear Dyn (2022) 110:431–448
https://doi.org/10.1007/s11071-022-07650-w

ORIGINAL PAPER

Approximate continuous fixed-time terminal sliding mode control with prescribed performance for uncertain robotic manipulators

Huayang Sai · Zhenbang Xu · Chengkai Xia · Xiangyang Sun

Received: 28 February 2022 / Accepted: 15 June 2022 / Published online: 29 June 2022

Abstract This paper studies an approximate continuous fixed-time terminal sliding mode control (CFTSMC) with prescribed performance for uncertain robotic manipulators. A transformation concerning tracking error using a fixed-time prescribed performance function is proposed to guarantee the transient and steady-state performance of trajectory tracking control for uncertain robotic manipulators within fixed time. Utilizing the transformed error, a smooth fixed-time sliding mode surface is designed. Then, based on the proposed sliding mode surface, an approximate CFTSMC scheme is presented to achieve inherent chattering-free control for uncertain robotic manipulators. According to the Lyapunov stability theory, it is proved that the position tracking error can be bounded in the prescribed performance boundaries and globally converges to a defined small region within fixed time and then approaches exponentially to the origin. Several numerical simulation results demonstrate the effectiveness and superiority of the proposed control strategy for uncertain robotic manipulators.

Keywords Fixed-time control · Sliding mode control · Prescribed performance · Robotic manipulator

H. Sai · Z. Xu (✉) · C. Xia · X. Sun
CAS Key Laboratory of On-orbit Manufacturing and Integration for Space Optics System, Changchun Institute of Optics, Fine Mechanics and Physics, Chinese Academy of Sciences, Changchun 130033, China
e-mail: xuzhenbang@ciomp.ac.cn

H. Sai
e-mail: saihuayang18@mails.ucas.ac.cn

C. Xia
e-mail: xiachengkai19@mails.ucas.ac.cn

X. Sun
e-mail: sunxiangyang19@mails.ucas.ac.cn

H. Sai · C. Xia · X. Sun
University of Chinese Academy of Sciences, Beijing 100049, China

1 Introduction

Achieving fast and high-precision trajectory tracking of multi-joint robotic manipulators has been a challenging objective due to the difficulty of obtaining accurate dynamic models and external disturbances that always significantly degrade the performance of robotic systems. Among many control algorithms, sliding mode control (SMC) has gotten much attention in virtue of its fast global convergence, simple implementation, order reduction, insensitivity to external disturbances and model errors, and changes in system parameters. Up to now, SMC and related technologies have been widely used in robotic systems [1–3].

For the conventional SMC schemes, a linear hyperplane-based sliding manifold is utilized to force the tracking error to the origin asymptotically in infinite time. A major weakness of the traditional SMC method is that only asymptotic convergence of the tracking error is guaranteed. However, in most robotic manipulator tracking applications, the tracking error of the

system is required to converge in a finite time. As a typical finite-time SMC method, the terminal sliding mode control (TSMC) can achieve finite-time convergence of the tracking error. In [4], TSMC was used to achieve finite-time tracking of robotic manipulators but lacked a reasonable consideration of system disturbances. Subsequently, several methods based on the TSMC have been derived to improve the control performance [5–7]. For example, to avoid singularities and achieve fast convergence of the system states far from the origin, a nonsingular TSMC scheme in [6] and a nonsingular fast terminal sliding mode control (NFTSMC) scheme [7] were developed, respectively. Another main weakness of traditional SMC applications is its strong chattering, which significantly affects the tracking control performance of robotic manipulators. To attenuate the chattering caused by the discontinuous symbol, some methods such as the boundary layer approach [8], integral SMC [9], and adaptive technology [10,11] have been proposed.

Despite the above advancements, the settling time of the finite-time control is hard to obtain due to its dependence on the initial states of the system, which prohibits their applications because the knowledge of initial conditions is always unavailable in advance. For example, in industrial production, the preset stabilization time is significant for the process planning of manufacturing [12,13]. In response, Polyakov [14] introduced a fixed-time control method to ensure a bounded convergence time independent of initial states. Then, some critical theoretical and mathematical analyses related to the fixed-time stability and convergence were presented, which facilitated the development and application of the fixed-time SMC [15–17]. Benefiting from the advantages that the settling time depends only on the defined parameters and is unrelated to the initial states, the fixed-time SMC has been widely applied to the attitude stabilization of spacecraft [18,19] and the control of multi-intelligent body systems [20,21]. For tracking control of robotic manipulators, the fixed-time SMC has also received extensive attention from scholars in recent years. For example, Xu [22] proposed an adaptive fixed-time control using universal barrier functions to address the problem of asymmetric output constraint of robotic manipulators. Su et al. [23] designed a novel fixed-time sliding surface for uncertain robotic manipulators, but the control torque suffers from strong chattering when the tracking error reaches the sliding phase. Zhang et al. [24] designed a continuous fixed-time SMC scheme, but at the expense of convergence speed and requiring a large initial torque. Sai et al. [25] proposed an adaptive fixed-time SMC scheme for uncertain robotic manipulators to attenuate chattering but also required a large initial control torque.

Common to the above contributions is the focus on the steady-state behavior of the system. However, the transient performance of the tracking error also significantly impacts the manipulation of many industrial control systems. On the one hand, funnel control was proposed to guarantee prescribed transient behavior, but its application objects were pretty limited [26,27]. On the other hand, Bechlioulis and Rovithakis [28] pioneered the use of the prescribed performance function (PPF) to bound the convergence error and the minimum convergence rate of the system. Subsequently, the prescribed performance control (PPC) technology was widely used in various classes of nonlinear systems to obtain the prescribed performance bounds (PPB) [29,30]. In particular, Karayiannidis et al. [31] and Jing et al. [32] exploited such a promising technique to investigate robust controller design in robotic manipulator trajectory tracking. In [33], the fixed-time SMC method in [23] was used in combination with the PPF technique, but there was unavoidable chattering in the control torque. It is worth noting that almost all PPFs guarantee only asymptotic or finite-time stability [34,35], which prevents its integration with the fixed-time control technology.

Driven by practical requirements for the uncertain robotic manipulators tracking control and inspired by previous discussions, we investigate a novel fixed-time TSMC combined with the prescribed performance method for uncertain robotic manipulators. The main contributions of this paper are twofold. First, a novel fixed-time PPF is designed to guarantee fixed-time convergence of the preset performance. Then, a fixed-time sliding surface is artfully constructed, and an approximate continuous fixed-time terminal sliding mode control (CFTSMC) scheme is proposed based on the designed sliding mode surface and the fixed-time PPF. The proposed controller can ensure that the system converges to a defined small region within fixed time and then goes to the origin exponentially, and also guarantees the transient performance of the system. The approximate fixed-time prescribed performance stability and the continuity of the control torque are demonstrated, respectively. Compared with existing SMC

schemes, the proposed scheme has the advantages of high tracking accuracy, low energy consumption, and chattering-free.

This paper is structured as follows: In Sect. 2, some problem statements and preliminaries are provided. The main of this work is proposed in Sect. 3, including the fixed-time PPF, the controller design, and stability analysis. Section 4 introduces two sets of numerical simulation results. Comparative study and discussion of quantification are given in Sect. 5, and some conclusions are drawn in Sect. 6.

2 Problem statement and preliminaries

2.1 Statement of notations

In this paper, $\|\boldsymbol{A}\| = tr\left(\boldsymbol{A}^T\boldsymbol{A}\right)$ and $\|\boldsymbol{x}\| = \sqrt{\boldsymbol{x}^T\boldsymbol{x}}$ represent the norm of the matrix $\boldsymbol{A} \in \mathbb{R}^{n\times n}$ and the vector $\boldsymbol{x} = [x_1, \cdots, x_n]^T$, respectively. $|\cdot|$ denotes the absolute value in $\mathbb{R}$. $\lambda_{\min}\{\boldsymbol{A}\}$ and $\lambda_{\max}\{\boldsymbol{A}\}$ are the minimum and maximum eigenvalues of the matrix $\boldsymbol{A}$. $\operatorname{sgn}(x)$ represents the signum function and the nonlinear function $\operatorname{sig}^{\alpha}(x)$ and vector $\mathbf{Sig}^{\alpha}(\boldsymbol{x}) \in \mathbb{R}^n$ are

$$\operatorname{sig}^{\alpha}(x) = |x|^{\alpha}\operatorname{sgn}(x), \tag{1}$$

$$\mathbf{Sig}^{\alpha}(\boldsymbol{x}) = \left[|x_1|^{\alpha}\operatorname{sgn}(x_1), \cdots, |x_n|^{\alpha}\operatorname{sgn}(x_n)\right]^T, \tag{2}$$

with $\alpha > 0$.

2.2 Some definitions and lemmas

Consider an autonomous dynamical system as:

$$\dot{\boldsymbol{x}} = \boldsymbol{f}(\boldsymbol{x}, \boldsymbol{\rho}), \tag{3}$$

where $\boldsymbol{x} \in \mathbb{R}^n$ is the system state, and the vector $\boldsymbol{\rho} \in \mathbb{R}^n$ stands for the tunable parameters of (3). The function $\boldsymbol{f} : \mathbb{R}^n \to \mathbb{R}^n$ is nonlinear and continuous, with $\boldsymbol{f}(0, \boldsymbol{\rho}) = 0$, and the initial state is $\boldsymbol{x}_0 = \boldsymbol{x}(0) \in \mathbb{R}^n$.

Definition 1 (Finite-time stability [36]) The origin of (3) is globally finite-time stable if it is globally asymptotically stable and any solution $\boldsymbol{x}(t, \boldsymbol{x}_0)$ of (3) reaches the equilibrium point at some finite-time moment, i.e., $\forall t \geqslant T(\boldsymbol{x}_0) : x(t, \boldsymbol{x}_0) = 0$, where $T : \mathbb{R}^n \to \mathbb{R}_+ \cup \{0\}$ is the settling-time function.

Definition 2 (Fixed-time stability [14]) The origin of (3) is globally fixed-time stable if it is globally finite-time stable and the settling-time function $T : \mathbb{R}^n \to \mathbb{R}_+ \cup \{0\}$ is bounded, i.e., $\exists T_{\max} > 0 : \forall \boldsymbol{x}_0 \in \mathbb{R}^n : T(\boldsymbol{x}_0) \leqslant T_{\max}$.

Definition 3 (Predefined-time stability [37]) For parameter vector $\boldsymbol{\rho}$ of (3) and a constant $T_c := T_c(\boldsymbol{\rho}) > 0$, the origin of (3) is predefined-time stable if it is fixed-time stable and the settling-time function $T : \mathbb{R}^n \to \mathbb{R}$ is such that

$$T(\boldsymbol{x}_0) \leqslant T_c, \forall \boldsymbol{x}_0 \in \mathbb{R}^n. \tag{4}$$

In this case, T_c is called as a predefined time.

Lemma 1 *[14] For the nonlinear system (3), if there exists a positive-definite continuous function $V(\xi) : U \to \mathbb{R}^n$ and positive constants $\alpha, \beta > 0, 0 < p < 1$ and $q > 1$ satisfying the inequality $\dot{V}(\xi) + \alpha V^p(\xi) + \beta V^q(\xi) < 0, \xi \in U\backslash\{0\}$, the system (3) is globally fixed-time stable with a settling time T bounded by*

$$T < T_{\max} = \frac{1}{\alpha(1-p)} + \frac{1}{\beta(q-1)}. \tag{5}$$

Lemma 2 *For a positive constant α and continuously differentiable x, the following equations hold:*

$$\frac{d|x|^{\alpha+1}}{dx} = (\alpha+1)|x|^{\alpha}sgn(x) \tag{6}$$

$$\frac{d\left(|x|^{\alpha+1}sgn(x)\right)}{dx} = (\alpha+1)|x|^{\alpha}. \tag{7}$$

The proof of Lemma 2 is given in "Appendix A".

Lemma 3 *[15] For constants $\xi_1, \xi_2, \cdots, \xi_n \geqslant 0$ and a positive constant p, the following inequalities hold*

$$\sum_{i=1}^{n}\xi_i^p \geqslant \left(\sum_{i=1}^{n}\xi_i\right)^p \quad \text{if } 0 < p \leqslant 1 \tag{8}$$

$$\sum_{i=1}^{n}\xi_i^p \geqslant n^{1-p}\left(\sum_{i=1}^{n}\xi_i\right)^p \quad \text{if } 1 < p < \infty. \tag{9}$$

Lemma 4 *[38] if $f(x)$ and $g(x)$ are two continuous function at $x_0 \in \mathbb{R}^n$, then the function $f(x) + g(x)$ is also continuous at x_0.*

2.3 Dynamic model of robotic manipulators

The dynamic model of a general n-degree-of-freedom (DOF) rigid robotic manipulator can be expressed as:

$$\boldsymbol{M}(\boldsymbol{q})\ddot{\boldsymbol{q}} + \boldsymbol{C}(\boldsymbol{q},\ \dot{\boldsymbol{q}})\dot{\boldsymbol{q}} + \boldsymbol{G}(\boldsymbol{q}) = \boldsymbol{\tau} + \boldsymbol{\tau}_d, \tag{10}$$

where $\boldsymbol{q},\ \dot{\boldsymbol{q}},\ \ddot{\boldsymbol{q}} \in \mathbb{R}^n$ represent the joint position, velocity, and acceleration vector of the robotic manipulator, respectively. $\boldsymbol{M}(\boldsymbol{q}) \in \mathbb{R}^{n\times n}$ is the symmetric and positive-definite matrix, $\boldsymbol{C}(\boldsymbol{q},\ \dot{\boldsymbol{q}}) \in \mathbb{R}^{n\times n}$ is the centrifugal-Coriolis matrix, and $\boldsymbol{G}(\boldsymbol{q}) \in \mathbb{R}^n$ is the Cartesian gravitational term. $\boldsymbol{\tau} \in \mathbb{R}^n$ is the vector of control input torque, and $\boldsymbol{\tau}_d \in \mathbb{R}^n$ represents an unknown but bounded external disturbance. The position error $\boldsymbol{e} \in \mathbb{R}^n$ and the velocity error $\dot{\boldsymbol{e}} \in \mathbb{R}^n$ are denoted as:

$$\boldsymbol{e} = \boldsymbol{q} - \boldsymbol{q}_d, \dot{\boldsymbol{e}} = \dot{\boldsymbol{q}} - \dot{\boldsymbol{q}}_d, \tag{11}$$

where $\boldsymbol{q}_d, \dot{\boldsymbol{q}}_d \in \mathbb{R}^n$ are vectors of the desired tracking angular position and velocity. The desired joint performance can be described as: [28]

$$\underline{b}_i \rho_i(t) < e_i(t) < \bar{b}_i \rho_i(t), \tag{12}$$

where $\rho_i(t)$ is the PPF given in the next section. $\underline{b}_i$ and $\bar{b}_i$ can be denoted, respectively, as:

$$\underline{b}_i = \begin{cases} -\vartheta_i, e_i(0) \geqslant 0 \\ -1, e_i(0) < 0 \end{cases}, \bar{b}_i = \begin{cases} 1, e_i(0) \geqslant 0 \\ \vartheta_i, e_i(0) < 0 \end{cases} \tag{13}$$

with $0 < \vartheta_i < 1$ is the overshoot index constant, $e_i(t), i = 1, \cdots, n$ is the ith element of the vector $\boldsymbol{e}$, and $e_i(0)$ is the initial joint angular position error of the joint i.

It is reasonable to postulate that the dynamics of robotic manipulators have the following propositions:

Proposition 1 *[39] The matrices $\boldsymbol{M}(\boldsymbol{q})$, $\boldsymbol{C}(\boldsymbol{q},\dot{\boldsymbol{q}})$ and $\boldsymbol{G}(\boldsymbol{q})$ can be described as:*

$$\begin{cases} \boldsymbol{M}(\boldsymbol{q}) = \boldsymbol{M}_0(\boldsymbol{q}) + \Delta\boldsymbol{M}(\boldsymbol{q}) \\ \boldsymbol{C}(\boldsymbol{q},\dot{\boldsymbol{q}}) = \boldsymbol{C}_0(\boldsymbol{q},\dot{\boldsymbol{q}}) + \Delta\boldsymbol{C}(\boldsymbol{q},\dot{\boldsymbol{q}}) \\ \boldsymbol{G}(\boldsymbol{q}) = \boldsymbol{G}_0(\boldsymbol{q}) + \Delta\boldsymbol{G}(\boldsymbol{q}), \end{cases} \tag{14}$$

where $\boldsymbol{M}_0(\boldsymbol{q})$, $\boldsymbol{C}_0(\boldsymbol{q},\dot{\boldsymbol{q}})$ and $\boldsymbol{G}_0(\boldsymbol{q})$ are nominal parts of the model parameters, and $\Delta\boldsymbol{M}(\boldsymbol{q})$, $\Delta\boldsymbol{C}(\boldsymbol{q},\dot{\boldsymbol{q}})$ and $\Delta\boldsymbol{G}(\boldsymbol{q})$ denote the system uncertainties.

Proposition 2 *[39] The matrices $\boldsymbol{M}(\boldsymbol{q})$, $\boldsymbol{C}(\boldsymbol{q},\dot{\boldsymbol{q}})$ and $\boldsymbol{G}(\boldsymbol{q})$ are bounded by*

$$M_m \leqslant \| \boldsymbol{M}(\boldsymbol{q}) \| \leqslant M_M, \text{ for } \forall \boldsymbol{q} \in \mathbb{R}^n \tag{15}$$

$$\| \boldsymbol{C}(\boldsymbol{q},\dot{\boldsymbol{q}}) \| \leqslant C_M \| \dot{\boldsymbol{q}} \|, \text{ for } \forall \boldsymbol{q},\dot{\boldsymbol{q}} \in \mathbb{R}^n \tag{16}$$

$$\| \boldsymbol{G}(\boldsymbol{q}) \| \leqslant G_M, \text{ for } \forall \boldsymbol{q} \in \mathbb{R}^n, \tag{17}$$

where M_m, M_M, C_M and G_M are known positive constants.

Lemma 5 *[40] In view of (10) and (14), the coupled uncertainty $\boldsymbol{\rho}(t)$ includes the external disturbance and system uncertainties, which can be written as:*

$$\boldsymbol{\rho}(t) = -\Delta\boldsymbol{M}(\boldsymbol{q})\ddot{\boldsymbol{q}} - \Delta\boldsymbol{C}(\boldsymbol{q},\dot{\boldsymbol{q}})\dot{\boldsymbol{q}} - \Delta\boldsymbol{G}(\boldsymbol{q}) + \boldsymbol{\tau}_d. \tag{18}$$

Then, the coupled uncertainty $\boldsymbol{\rho}(t)$ can be bounded with

$$\| \boldsymbol{\rho}(t) \| < b_0 + b_1 \| \boldsymbol{q}(t) \| + b_2 \| \dot{\boldsymbol{q}}(t) \|^2 + \gamma \| \boldsymbol{\tau} \|. \tag{19}$$

Our goal is to design an approximate fixed-time controller—to force the joint tracking error of the robot to converge to a defined small neighborhood within fixed time unrelated to the initial states, with prescribed performance.

3 Control development and analysis

3.1 Fixed-time prescribed performance function design

According to the prescribed performance (12), the tracking error $e(t)$ is required to evolve strictly in the designed set of residuals. It means that the convergence rate is not less than a preset value, exhibiting maximum overshoot less than a preallocated constant. The critical to satisfying the prescribed performance requirements is to make the control performance of the system satisfy (12) with the aid of the fixed-time PPF. First, the definition of the PPF is given as:

Definition 4 [28] A smooth function $\rho : \mathbb{R}_+ \to \mathbb{R}_+$ will be called a PPF if:

1. ρ is positive and decreasing;
2. $\lim_{t\to\infty} \rho(t) = \rho_\infty > 0$.

Then, to ensure that the PPF is fixed-time stable, a novel fixed-time PPF is designed as:

$$\rho_i(t) = \begin{cases} (\rho_{0i} - \rho_{\infty i})\left(1 - \frac{t}{T_i}\right)^{\sigma_i} + \rho_{\infty i}, 0 \leqslant t < T_i \\ \rho_{\infty i}, t \geqslant T_i \end{cases}, \tag{20}$$

where $0 < \rho_{\infty i} < |e_i(0)| < \rho_{0i}$, $T_i > 0$ and $\sigma_i > 2$ are defined positive constants. The constant T_i is the preset maximum settling time for $\rho_i(t)$ converging from the maximum initial error ρ_{0i} to the maximum allowable steady-state error $\rho_{\infty i}$, and $\dot{\rho}_i(t)$ denotes the prespecified minimum convergence rate.

Proposition 3 *The proposed fixed-time PPF* (20) *satisfies*

1. *$\rho_i(t)$ is a monotone decreasing bounded smooth positive function, such that $0 < \rho_{\infty i} \leqslant \rho_i(t) \leqslant \rho_{0i}$ and $\dot{\rho}_i(t) \leqslant 0$;*
2. *$\lim_{t\to T_i} \rho_i(t) = \rho_{\infty i}$ and $\rho_i(t) = \rho_{\infty i}$ for $t \geqslant T_i$.*

The proof of Proposition 3 is given in "Appendix B."

Remark 1 The preceding discussion can be summarized that $\rho_i(t)$ in (20) can converge to $\rho_{\infty i}$ with the preset time T_i. However, the conventional exponential performance function in [28,31,41,42] only can guarantee convergence to a given range when time tends to infinity. Besides, the finite-time performance function in [43] can guarantee it converge to a given range in a finite time, but the convergence time depends on the initial value of the function. In comparison, the convergence of the proposed fixed-time PPF is only related to the parameter T_i, and the form is more concise than that in [33,44].

An example of $\rho_i(t)$ shown in Fig. 1 to illustrate the fixed-time convergence of the proposed function (20) with different initial values $\rho_{0i} = 0.5,\ 100$ and different convergence time $T_i = 2,\ 5$, and the other parameters are given as $\rho_{\infty i} = 0.01,\ \sigma_i = 2.01$. It can obtain that $\rho_i(t)$ can converge to the $\rho_{\infty i}$ within the given convergence time T_i for different ρ_{0i}.

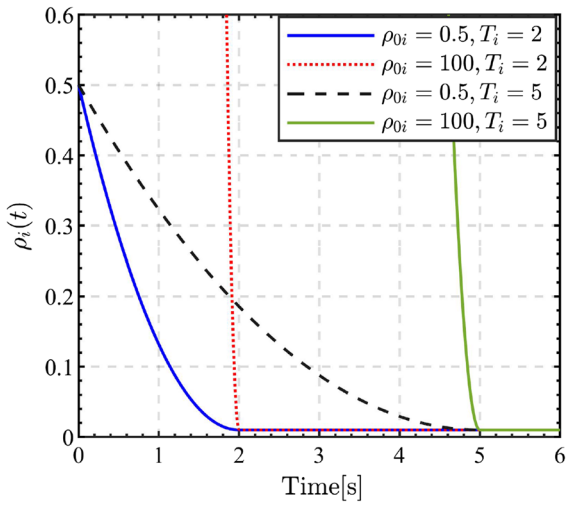

Fig. 1 Illustration of $\rho_i(t)$

Noting that (20) cannot be used directly to design the controller, an error transformation is required to establish the link between the tracking error and the fixed-time PPF. Considering the transformation function $\psi(x)$ as [33]:

$$\psi(x) = \frac{\underline{b}_i \bar{b}_i (\exp(x) - 1)}{\underline{b}_i \exp(x) - \bar{b}_i}, \tag{21}$$

we can declare that $\psi(x)$ satisfies:

Proposition 4 *1. $\psi(x)$ is a smooth and strictly increasing function;*

2. *$\lim_{x\to-\infty} \psi(x) = \underline{b}_i$ and $\lim_{x\to+\infty} \psi(x) = \bar{b}_i$;*
3. *With ε_{1i} being a transformed error and the error e_i being related to ε_{1i} by*

$$e_i = \rho_i \psi(\varepsilon_{1i}), \tag{22}$$

then, the prescribed performance (12) *can be guaranteed.*

The proof of Proposition 4 is given in "Appendix C".

By Property 4, it is noted that $\rho_i \psi(\varepsilon_{1i}) \in (b_i \rho_i, \bar{b}_i \rho_i)$. Therefore, the tracking error e_i can be replaced by ε_{1i} through an inverse transformation, thus ensuring that the system performance satisfies (12), which is a common method in PPC technology. The inverse function of $\psi(x)$ can be calculated as:

$$\psi^{-1}(x) = \ln\left(\frac{\bar{b}_i\left(x - \underline{b}_i\right)}{-\underline{b}_i\left(\bar{b}_i - x\right)}\right). \tag{23}$$

From Proposition 4, it can obtain that $\psi^{-1}(x)$ is a smooth function, increasing bijective mapping with $\lim_{\varepsilon_{1i}\to\bar{b}_i} \psi^{-1}(\varepsilon_{1i}) = \infty$ and $\lim_{\varepsilon_{1i}\to\underline{b}_i} \psi^{-1}(\varepsilon_{1i}) = -\infty$.

According to (22), $\psi(\varepsilon_{1i})$ and the transformed error ε_{1i} can be written as:

$$\psi(\varepsilon_{1i}) = \frac{e_i}{\rho_i},\ \varepsilon_{1i} = \psi^{-1}\left(\frac{e_i}{\rho_i}\right). \tag{24}$$

Then, the time derivative of ε_{1i} in (24) is

$$\dot{\varepsilon}_{1i} = \beta_i\left(\dot{e}_i + \alpha_i e_i\right), \tag{25}$$

where α_i and β_i represent as:

$$\alpha_i = -\dot{\rho}_i/\rho_i, \beta_i = v\left(\frac{e_i}{\rho_i}\right)/\rho_i, \tag{26}$$

and $v(x)$ represents the derivative of $\psi^{-1}(x)$ with respect to x as:

$$v(x) = \dot{\psi}^{-1}(x) = \frac{1}{x - \underline{b}_i} + \frac{1}{\bar{b}_i - x}. \tag{27}$$

From (25), the vector $\dot{\boldsymbol{\varepsilon}}_1$ and its derivative can be denoted as:

$$\begin{cases} \dot{\boldsymbol{\varepsilon}}_1 = \boldsymbol{\varepsilon}_2 = \boldsymbol{B}\left(\dot{\boldsymbol{e}} + \boldsymbol{A}\boldsymbol{e}\right) \\ \dot{\boldsymbol{\varepsilon}}_2 = \boldsymbol{B}\left(\ddot{\boldsymbol{e}} + \dot{\boldsymbol{A}}e + \boldsymbol{A}\dot{\boldsymbol{e}}\right) \end{cases}, \tag{28}$$

where $\boldsymbol{A} = \mathrm{diag}(\alpha_1, \cdots, \alpha_n)$ is a semipositive definite diagonal matrix and $\boldsymbol{B} = \mathrm{diag}(\beta_1, \cdots, \beta_n)$ is a positive definite diagonal matrix. To facilitate the proof subsequently, a proposition is declared in advance as:

Proposition 5 *α_i and β_i in (26) satisfy $\alpha_i \geqslant 0$ and $\beta_i > 2\rho_{0i}^{-1}$.*

The proof of Proposition 5 is given in "Appendix D".

3.2 Fixed-time terminal sliding mode surface design

First, a smooth nonlinear function $s^p(x) \in \mathcal{C}^1$ is designed as:

$$s^p(x) = \begin{cases} \mathrm{sig}^p(x), |x| \geqslant \delta \\ l_1 x + l_2 \mathrm{sig}^2(x) + l_3 x^3, |x| < \delta \end{cases}, \tag{29}$$

where p and δ represent the two defined positive constants satisfying $0 < p < 1$ and $0 < \delta \leqslant 1$. l_1, l_2 and l_3 are three constants about δ and p, which can be calculated with

$$l_1 = \left(\frac{1}{2}p^2 - \frac{5}{2}p + 3\right)\delta^{p-1} \tag{30}$$

$$l_2 = \left(-p^2 + 4p - 3\right)\delta^{p-2} \tag{31}$$

$$l_3 = \left(\frac{1}{2}p^2 - \frac{3}{2}p + 1\right)\delta^{p-3}. \tag{32}$$

With Lemma 2, the derivative of $s^p(x)$ with respect to x can be calculated as:

$$\dot{s}^p(x) = \begin{cases} p|x|^{p-1}, |x| \geqslant \delta \\ l_1 + 2l_2|x| + 3l_3x^2, |x| < \delta \end{cases}. \tag{33}$$

Then, another nonlinear function $s^q(x)$ is given as:

$$s^q(x) = \mathrm{sig}^q(x), \tag{34}$$

where $q > 1$ is a defined positive constant. The derivative of $s^q(x)$ with respect to x can be written as:

$$\dot{s}^q(x) = q|x|^{q-1}. \tag{35}$$

To simplify the design and analysis of the sliding surface and the controller, define the following vectors and matrices as:

$$\boldsymbol{S}^p(\boldsymbol{x}) = \left[s^p(x_1), \cdots, s^p(x_n)\right]^T \tag{36}$$

$$\boldsymbol{F}^p(\boldsymbol{x}) = \mathrm{diag}\left(\dot{s}^p(x_1), \cdots, \dot{s}^p(x_n)\right) \tag{37}$$

$$\boldsymbol{S}^q(\boldsymbol{x}) = \left[s^q(x_1), \cdots, s^q(x_n)\right]^T \tag{38}$$

$$\boldsymbol{H}^q(\boldsymbol{x}) = \mathrm{diag}\left(\dot{s}^q(x_1), \cdots, \dot{s}^q(x_n)\right). \tag{39}$$

Based on the vectors $\boldsymbol{S}^p(\boldsymbol{x})$ and $\boldsymbol{S}^q(\boldsymbol{x})$, a fixed-time TSM surface is designed as:

$$\boldsymbol{s} = \boldsymbol{B}^{-1}\boldsymbol{\varepsilon}_2 + \boldsymbol{K}_1\boldsymbol{S}^p(\boldsymbol{\varepsilon}_1) + \boldsymbol{K}_2\boldsymbol{S}^q(\boldsymbol{\varepsilon}_1), \tag{40}$$

where vectors $\boldsymbol{\varepsilon}_1$ and $\boldsymbol{\varepsilon}_2$ are defined in (24) and (28), and $\boldsymbol{K}_1, \boldsymbol{K}_2 \in \mathbb{R}^{n\times n}$ are two diagonal positive definite matrices.

Remark 2 Different from $\boldsymbol{e}$ and $\dot{\boldsymbol{e}}$ used in [23], the proposed sliding surface replaces them by $\boldsymbol{\varepsilon}_1$ and $\boldsymbol{\varepsilon}_2$. The advantage of the proposed sliding surface is that it can guarantee that the position error satisfies the PPB in (12) and can converge to a defined small region within fixed time. Moreover, unlike in [33] where only the $\boldsymbol{e}$ and $\dot{\boldsymbol{e}}$ of the sliding surface in [23] are replaced, the proposed nonlinear function $s^p(x)$ used in the proposed sliding surface is continuous and smooth, and has a faster convergence rate.

3.3 Approximate continuous fixed-time terminal sliding mode controller design

Based on the proposed fixed-time sliding surface, a nonsingular approximate continuous fixed-time terminal sliding mode prescribed performance control (CFTSMPPC) is designed as:

$$\boldsymbol{\tau} = \boldsymbol{\tau}_0 + \boldsymbol{\tau}_1 + \boldsymbol{\tau}_2 \tag{41}$$

with

$$\boldsymbol{\tau}_0 = \boldsymbol{M}_0(\boldsymbol{q})\left(\ddot{\boldsymbol{q}}_{\boldsymbol{d}} - \dot{\boldsymbol{A}}\boldsymbol{e} - \boldsymbol{A}\dot{\boldsymbol{e}}\right) + \boldsymbol{C}_0(\boldsymbol{q},\dot{\boldsymbol{q}})\dot{\boldsymbol{q}} + \boldsymbol{G}_0(\boldsymbol{q}) \tag{42}$$

$$\boldsymbol{\tau}_1 = -\boldsymbol{K}_0\mathbf{Sig}^r(\boldsymbol{s}) - \boldsymbol{M}_0(\boldsymbol{q})\left(\boldsymbol{K}_1\boldsymbol{F}^p(\boldsymbol{\varepsilon}_1) + \boldsymbol{K}_2\boldsymbol{H}^q(\boldsymbol{\varepsilon}_1)\right)\boldsymbol{\varepsilon}_2 \tag{43}$$

$$\boldsymbol{\tau}_2 = -u\frac{\boldsymbol{s}}{\|\boldsymbol{s}\|} \tag{44}$$

and

$$u = \frac{1}{1-\gamma}\left(k + b_0 + b_1\|\boldsymbol{q}\| + b_2\|\dot{\boldsymbol{q}}\|^2 + \gamma\|\boldsymbol{\tau}_0 + \boldsymbol{\tau}_1\|\right), \tag{45}$$

where $\boldsymbol{K}_0 \in \mathbb{R}^{n\times n}$ is a given positive-definite symmetric matrix, $r > 1$ and $k > 0$ are two positive gains. b_0, b_1, b_2 and γ are positive constants, and γ is given by

$$\gamma = \frac{m_2 - m_1}{m_2 + m_1}, \tag{46}$$

where m_1 and m_2 are two positive constants satisfying

$$m_1 \leqslant \left\|\boldsymbol{M}^{-1}(\boldsymbol{q})\right\| \leqslant m_2. \tag{47}$$

Theorem 1 *With the uncertain robotic manipulator system (10) and the proposed CFTSMPPC in (41)-(45), the following three facts hold true.*

1. *The transformed error ε_{1i} globally converges to an arbitrary small set $R_\delta = \{\varepsilon_{1i}\,|\,|\varepsilon_{1i}| \leqslant \delta\}$ with the settling time T and then goes zero exponentially. The upper bound of the settling time $T_{\max}$ includes the reaching time T_r and the sliding time T_s. The reaching time T_r is the period that the tracking trajectory converges globally to the sliding mode surface, and the sliding time T_s denotes the period in which the tracking error converges to a defined small domain of the origin. T, T_r and T_s can be described by the following equalities:*

$$T \leqslant T_{\max} = T_r + T_s \tag{48}$$

$$T_r \leqslant \frac{2}{k(m_1+m_2)^{\frac{1}{2}}} + \frac{2}{n^{\frac{1-r}{2}}\lambda_{\min}(\boldsymbol{K}_0)(m_1+m_2)^{\frac{r+1}{2}}(r-1)} \tag{49}$$

$$T_s \leqslant \frac{2^{-\frac{p+1}{2}}\rho_{0i}}{k_{1i}(1-p)} + \frac{2^{-\frac{q+1}{2}}\rho_{0i}}{k_{2i}(q-1)}. \tag{50}$$

2. *The position tracking error e_i can remain within the prescribed performance boundaries in (12) and converge to the prescribed stable region $R_b = \left\{e_i\,|, \underline{b}_i\rho_{\infty i} < e_i < \bar{b}_i\rho_{\infty i}\right\}$ within T_i in (20), and then keeps within the region.*
3. *Generally, the boundary layer method [8] can be applied to eliminate chattering in $\boldsymbol{\tau}_2$. Therefore, (44) can be modified as:*

$$\boldsymbol{\tau}_2 = -u\frac{\boldsymbol{s}}{\|\boldsymbol{s}\| + s_0}, \tag{51}$$

where s_0 is a small positive constant. Then, the control torque of the proposed CFTSMPPC can be regarded continuous and chattering-free, i.e., for any moment, it has $\lim_{t\to t^-}\boldsymbol{\tau} = \lim_{t\to t^+}\boldsymbol{\tau}$.

Proof First, the proof of Theorem 1 (1) is given. The stability analysis of the proposed CFTSMPPC scheme can be divided into the reaching phase and the sliding phase.

Step 1. In the reaching phase, with (36)-(39) and the sliding surface (40), $\boldsymbol{M}_0(\boldsymbol{q})\dot{\boldsymbol{s}}$ can be derived as:

$$\boldsymbol{M}_0(\boldsymbol{q})\dot{\boldsymbol{s}} = \boldsymbol{B}^{-1}\boldsymbol{M}_0(\boldsymbol{q})\dot{\boldsymbol{\varepsilon}}_2 + \boldsymbol{M}_0(\boldsymbol{q}) \left(\boldsymbol{K}_1\boldsymbol{F}^p(\boldsymbol{\varepsilon}_1) + \boldsymbol{K}_2\boldsymbol{H}^q(\boldsymbol{\varepsilon}_1)\right)\boldsymbol{\varepsilon}_2. \tag{52}$$

Considering $\dot{\boldsymbol{\varepsilon}}_2$ in (28) and the dynamic model in (10), $\boldsymbol{M}_0(\boldsymbol{q})\dot{\boldsymbol{\varepsilon}}_2$ can be obtained by

$$\boldsymbol{M}_0(\boldsymbol{q})\dot{\boldsymbol{\varepsilon}}_2 = \boldsymbol{B}\left(\boldsymbol{\tau} + \boldsymbol{\rho} - \boldsymbol{C}_0(\boldsymbol{q},\dot{\boldsymbol{q}})\dot{\boldsymbol{q}} - \boldsymbol{G}_0(\boldsymbol{q})\right) + \boldsymbol{M}_0(\boldsymbol{q})\boldsymbol{B}\left(\dot{\boldsymbol{A}}\boldsymbol{e} + \boldsymbol{A}\dot{\boldsymbol{e}} - \ddot{\boldsymbol{q}}_{\boldsymbol{d}}\right). \tag{53}$$

Then, substituting (53) and the control law (41)-(45) in (52), we have

$$\boldsymbol{M}_0(\boldsymbol{q})\dot{\boldsymbol{s}} = -\frac{1}{1-\gamma}\left(k + b_0 + b_1\|\boldsymbol{q}\| + b_2\|\dot{\boldsymbol{q}}\|^2 + \gamma\|\boldsymbol{\tau}_0 + \boldsymbol{\tau}_1\|\right)\frac{\boldsymbol{s}}{\|\boldsymbol{s}\|} + \boldsymbol{\rho} - \boldsymbol{K}_0\mathbf{Sig}^r(\boldsymbol{s}). \tag{54}$$

The Lyapunov function can be defined as:

$$V_1 = \frac{1}{2}\boldsymbol{s}^T\boldsymbol{M}_0(\boldsymbol{q})\boldsymbol{s}. \tag{55}$$

Differentiating V_1 with respect to time yields

$$\begin{aligned}\dot{V}_1 &= \boldsymbol{s}^T\boldsymbol{M}_0(\boldsymbol{q})\dot{\boldsymbol{s}}\\ &= \boldsymbol{s}^T\left[-\frac{1}{1-\gamma}\left(k + b_0 + b_1\|\boldsymbol{q}\| + b_2\|\dot{\boldsymbol{q}}\|^2 + \gamma\|\boldsymbol{\tau}_0 + \boldsymbol{\tau}_1\|\right)\frac{\boldsymbol{s}}{\|\boldsymbol{s}\|} + \boldsymbol{\rho} - \boldsymbol{K}_0\mathbf{Sig}^r(\boldsymbol{s})\right]\\ &= -\frac{\|\boldsymbol{s}\|}{1-\gamma}\left(k + b_0 + b_1\|\boldsymbol{q}\| + b_2\|\dot{\boldsymbol{q}}\|^2 + \gamma\|\boldsymbol{\tau}_0 + \boldsymbol{\tau}_1\|\right) + \boldsymbol{s}^T\boldsymbol{\rho} - \boldsymbol{s}^T\boldsymbol{K}_0\mathbf{Sig}^r(\boldsymbol{s}).\end{aligned} \tag{56}$$

Substituting (45) in (56) leads to

$$\dot{V}_1 \leqslant -\gamma\|\boldsymbol{s}\|u - \|\boldsymbol{s}\|\left(k + b_0 + b_1\|\boldsymbol{q}\| + b_2\|\dot{\boldsymbol{q}}\|^2 + \gamma\|\boldsymbol{\tau}_0 + \boldsymbol{\tau}_1\|\right) + \|\boldsymbol{s}\|\|\boldsymbol{\rho}\| - \boldsymbol{s}^T\boldsymbol{K}_0\mathbf{Sig}^r(\boldsymbol{s}). \tag{57}$$

Considering the upper bound of the coupled uncertainty in (19), (57) can lead to

$$\dot{V}_1 \leqslant -\gamma\|\boldsymbol{s}\|u - k\|\boldsymbol{s}\| - \gamma\|\boldsymbol{s}\|\|\boldsymbol{\tau}_0 + \boldsymbol{\tau}_1\| + \gamma\|\boldsymbol{s}\|\|\boldsymbol{\tau}\| - \boldsymbol{s}^T\boldsymbol{K}_0\mathbf{Sig}^r(\boldsymbol{s}). \tag{58}$$

According to (41), we have

$$\|\boldsymbol{\tau}\| \leqslant \|\boldsymbol{\tau}_0 + \boldsymbol{\tau}_1\| + \|\boldsymbol{\tau}_2\|. \tag{59}$$

Then, substituting (59) in (58), it follows that

$$\begin{aligned}\dot{V}_1 &\leqslant -k\|\boldsymbol{s}\| - \boldsymbol{s}^T\boldsymbol{K}_0\mathbf{Sig}^r(\boldsymbol{s})\\ &\leqslant -k\|\boldsymbol{s}\| - \lambda_{\min}(\boldsymbol{K}_0)\left(\sum_{i=1}^{n}|s_i|^2\right)^{\frac{r+1}{2}}.\end{aligned} \tag{60}$$

In light of Lemma 3, (60) can lead to

$$\dot{V}_1 \leqslant -n^{\frac{1-r}{2}}\lambda_{\min}(\boldsymbol{K}_0)\|\boldsymbol{s}\|^{r+1} - k\|\boldsymbol{s}\|. \tag{61}$$

Due to the fact that $\boldsymbol{M}_0(\boldsymbol{q})$ can be chosen as [40]:

$$\boldsymbol{M}_0(\boldsymbol{q}) = \frac{2}{m_1 + m_2}\boldsymbol{I}_n, \tag{62}$$

V_1 can be written as:

$$V_1 = \frac{1}{m_1 + m_2}\|\boldsymbol{s}\|^2. \tag{63}$$

Then, combining with (63), (61) can be written as:

$$\dot{V}_1 + n^{\frac{1-r}{2}}\lambda_{\min}(\boldsymbol{K}_0)(m_1 + m_2)^{\frac{r+1}{2}}V^{\frac{r+1}{2}} + k(m_1 + m_2)^{\frac{1}{2}}V^{\frac{1}{2}} \leqslant 0. \tag{64}$$

As described in Lemma 1, and the fact $r > 1$, the sliding surface $\boldsymbol{s}$ can globally converge to zero with the reaching time T_r bounded by (49).

Step 2. In the reaching phase, the error convergence enters the sliding phase once the sliding surface reaches $\boldsymbol{s} = 0$, and (40) can lead to

$$\varepsilon_{2i} = -\beta_i\left(k_{1i}s^p(\varepsilon_{1i}) + k_{2i}s^q(\varepsilon_{1i})\right). \tag{65}$$

Since $s^p(\varepsilon_{1i})$ is a piecewise function of ε_{1i}, there are two cases for discussion.

Case 1. If $|\varepsilon_{1i}| \geqslant \delta$, (65) can be expressed as:

$$\varepsilon_{2i} = -\beta_i k_{1i} \mathrm{sig}^p(\varepsilon_{1i}) - \beta_i k_{2i} \mathrm{sig}^q(\varepsilon_{1i}). \tag{66}$$

The following Lyapunov function is considered as:

$$V_2 = \frac{1}{2}\varepsilon_{1i}^2. \tag{67}$$

Taking the first derivative of (67), it has

$$\dot{V}_2 = \varepsilon_{1i}\varepsilon_{2i} = -\beta_i k_{1i}|\varepsilon_{1i}|^{p+1} - \beta_i k_{2i}|\varepsilon_{1i}|^{q+1}. \tag{68}$$

Considering Proposition 5, (68) satisfies

$$\dot{V}_2 < -\rho_{0i}^{-1} k_{1i} 2^{\frac{p+3}{2}} V_2^{\frac{p+1}{2}} - \rho_{0i}^{-1} k_{2i} 2^{\frac{q+3}{2}} V_2^{\frac{q+1}{2}}. \tag{69}$$

By Lemma 1, in the sliding phase, the transformed error ε_{1i} can converge to an arbitrary small set R_δ within a fixed time T_s given in (50).

Case 2. If $|\varepsilon_{1i}| < \delta$, (65) can be written as:

$$\begin{aligned}\varepsilon_{2i} = &-\beta_i k_{1i}\left(l_1\varepsilon_{1i} + l_2\mathrm{sig}^2(\varepsilon_{1i}) + l_3\varepsilon_{1i}^3\right)\\ &-\beta_i k_{2i}\mathrm{sig}^q(\varepsilon_{1i}).\end{aligned} \tag{70}$$

Similarly, differentiating V_2 with respect to time and substituting (30)-(32) and (70) leads to

$$\begin{aligned}\dot{V}_2 &= -\beta_i k_{1i}\left(l_1\varepsilon_{1i}^2 + l_2|\varepsilon_{1i}|^3 + l_3\varepsilon_{1i}^4\right) - \beta_i k_{2i}|\varepsilon_{1i}|^{q+1}\\ &= -\beta_i k_{1i}\delta^{p-1}V_2\\ &\quad\left[\underbrace{\left(p^2-5p+6\right) - 2^{\frac{3}{2}}\delta^{-1}\left(p^2-4p+3\right)V_2^{\frac{1}{2}} + \left(2p^2-6p+4\right)\delta^{-2}V_2}_{f(V_2)}\right]\\ &\quad - 2^{\frac{q+1}{2}}\beta_i k_{2i}V_2^{\frac{q+1}{2}}.\end{aligned} \tag{71}$$

With $|\varepsilon_{1i}| < \delta$, we can have $0 \leqslant V_2 < \frac{1}{2}\delta^2$. Then, it is easy to obtain $f(V_2) > 0$, so (71) can yield

$$\dot{V}_2 < -2^{\frac{q+1}{2}}\beta_i k_{2i}V_2^{\frac{q+1}{2}} < 0. \tag{72}$$

According to the Lyapunov stability theory [8], the transformed error ε_{1i} can converge to zero exponentially when $|\varepsilon_{1i}| < \delta$. This completes the proof of Theorem 1 (1).

Then, the proof of Theorem 1 (2) is given as follows.

Based on the above analysis, and Proposition 3, we have $\psi(\varepsilon_{1i}) \in \left(\underline{b}_i, \bar{b}_i\right)$. From Proposition 4 (1), it has $\rho_i(t) = \rho_{\infty i}$ for $t \geqslant T_i$. Combined with $e_i = \rho_i\psi(\varepsilon_{1i})$ in (22), when $t \geqslant T_i$, the range of tracking error can be bounded with

$$e_i \in \left(\rho_{\infty i}\underline{b}_i, \rho_{\infty i}\bar{b}_i\right). \tag{73}$$

When $t < T_i$, the range of tracking error can be represented as (12). Hence, this completes the proof of Theorem 1 (2).

Finally, the proof of Theorem 1 (3) is given as follows.

According to Lemma 4, to prove that $\boldsymbol{\tau}$ in (41) is continuous, it is sufficient to show that (42), (43) and (51) are continuous functions. It is easy to obtain that $\boldsymbol{\tau}_0$ is always continuous for $\boldsymbol{e} \in \mathbb{R}^n$. $\boldsymbol{\tau}_1$ in (43) and $\boldsymbol{\tau}_2$ in (51) contain the vector consisting of the segment function $s^p(x)$ and its first-order derivative $\dot{s}^p(x)$. If $s^p(x)$ and its derivative $\dot{s}^p(x)$ both are continuous at $x = \delta$, we can have that $\boldsymbol{\tau}_1$ is continuous.

With $\delta > 0$ in (29) and (33), we can obtain

$$\lim_{x\to\delta^+} s^p(x) = \mathrm{sig}^p(\delta) = \delta^p \tag{74}$$

$$\begin{aligned}\lim_{x\to\delta^-} s^p(x) = &\left(\frac{1}{2}p^2 - \frac{5}{2}p + 3\right)\delta^p\\ &+\left(-p^2+4p-3\right)\delta^p\\ &+\left(\frac{1}{2}p^2 - \frac{3}{2}p + 1\right)\delta^p = \delta^p\end{aligned} \tag{75}$$

$$\lim_{x\to\delta^+} \dot{s}^p(x) = p|\delta|^{p-1} = p\delta^{p-1} \tag{76}$$

$$\lim_{x\to\delta^-}\dot{s}^p(x)=\left(\frac{1}{2}p^2-\frac{5}{2}p+3\right)\delta^{p-1}+2\left(-p^2+4p-3\right)\delta^{p-1}+3\left(\frac{1}{2}p^2-\frac{3}{2}p+1\right)\delta^{p-1}=p\delta^{p-1}. \tag{77}$$

Due to $\lim_{x\to\delta^+}s^p(x)=\lim_{x\to\delta^-}s^p(x)$ and $\lim_{x\to\delta^+}\dot{s}^p(x)=\lim_{x\to\delta^-}\dot{s}^p(x)$, we can obtain that $s^p(x)$ and $\dot{s}^p(x)$ is continuous at $x=\delta$. This completes the proof of Theorem 1 (3). □

Remark 3 In [23,33], a nonlinear function similar to the proposed $s^p(x)$ in $\boldsymbol{\tau}_1$ is expressed as:

$$\hat{s}^p(x)=\begin{cases}\mathrm{sig}^p(x), |x|\geqslant\delta\\ \delta^{p-1}x, |x|<\delta\end{cases}. \tag{78}$$

It is easy to calculate that the first-order derivative of $\hat{s}^p(x)$ is a discontinuous function, which can cause significant transient changes in the control torque and thus damage the controller. In contrast, the control torque of our proposed controller is continuous and chattering-free according to Theorem 1(3).

Remark 4 When the transformed error ε_{1i} tends to zero, i.e., $|\varepsilon_{1i}|<\delta$, it can be calculated that the value of the first derivative of $s^p(x)$ is larger than that of $\hat{s}^p(x)$. Therefore, the proposed controller can obtain a faster convergence rate to the neighborhood near the origin than fixed-time controllers in [23,33].

Remark 5 Compared to the finite-time controller in [4] without considering the uncertainty of the robotic manipulator and external disturbances, and some fixed-time controllers [23,24,33] regard the coupling uncertainty of the robotic manipulator bounded by

$$\|\hat{\boldsymbol{\rho}}(t)\|<b_0+b_2\|\dot{\boldsymbol{q}}(t)\|^2+\gamma\|\boldsymbol{\tau}\|, \tag{79}$$

the influence of the joint angle of the uncertain robotic manipulator on its dynamics model is fully considered in the proposed controller.

Remark 6 The proposed controller parameters should be carefully chosen by the following principles. The control parameters in PPF should satisfy $0<\rho_{\infty i}<|e_i(0)|<\rho_{0i}$, $T_i>0$ and $\sigma_i>2$, where the smaller T_i and the larger σ_i contribute to a faster convergence of the system, but too small T_i and too large σ_i may lead to actuator saturation or even instability. The value of σ_i has a significant effect on the controller, and it should be chosen close to 2. Then, constants m_1 and m_2 should be chosen to satisfy the inequality (47); otherwise, it can lead to torque chattering. After that, the other control parameters $\boldsymbol{K}_0, \boldsymbol{K}_1, \boldsymbol{K}_2, r>1, k>0, 0<p<1, 0<\delta\leqslant 1$ and $q>1$ should be chosen by trial-and-error for a good tracking performance. Generally, δ should be chosen as small as possible ensuring the convergence accuracy of the system as long as the control torque allows. Smaller p contributes to fast transient response, and q should be chosen as small as possible, they can have a large effect on the control torque and should be modified carefully. Larger control gains $\boldsymbol{K}_0, \boldsymbol{K}_1, \boldsymbol{K}_2$ and k contribute to faster convergence rates but result in larger control inputs, so a trade-off must be made between the control input and the control performance.

4 Simulation results

In this section, two simulation examples are used to demonstrate the effectiveness and advantages of the proposed controller. First, a two-link robotic manipulator is considered to illustrate the contribution of the proposed controller in eliminating chattering and constraining tracking errors. In the second example, a more complex 3-DOF robotic manipulator is considered to illustrate the robustness of the proposed control scheme against disturbances and other advantages by comparing it with several different SMC schemes. In both simulation examples, the proposed CFTSMPPC use the modified continuous controller in (51). All the simulations are conducted using the Simulink of MATLAB R2020a, with a time step size of 1×10^{-4} s.

Example 4.1 Considering a two-link robotic manipulator depicted in Fig. 2, and being affected by the gravity field [45].

The dynamic parameters of the two-link robotic manipulator are chosen as: $l_1=1$ m, $l_2=0.8$ m, $m_1=0.5$ kg, $m_2=1.5$ kg, $I_1=I_2=5$ kg $\cdot$ m^2, where l_i, m_i and I_i denote the length, mass, and inertia of the link i, respectively, and $g=9.8$ m/s^2 is the acceleration of gravity. Considering the uncertainty of dynamic model, the nominal values are set as $m_1^0=0.6$ kg, $m_2^0=1.8$ kg and $I_1^0=I_2^0=$

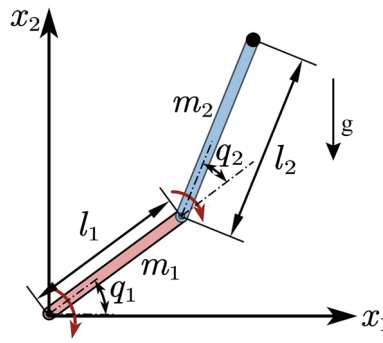

Fig. 2 Schematic of the two-link rigid robotic manipulator

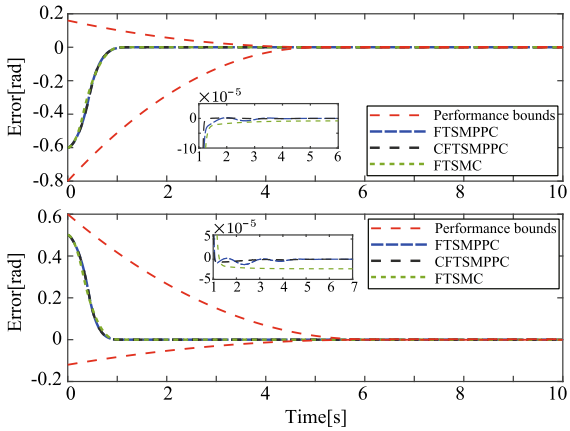

Fig. 3 Position tracking errors

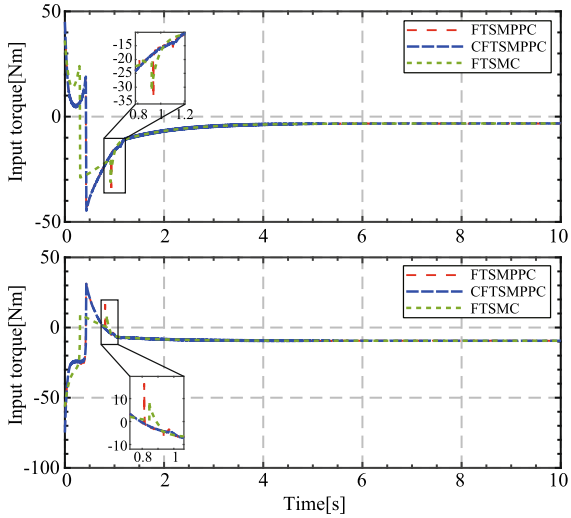

Fig. 4 Control input torque

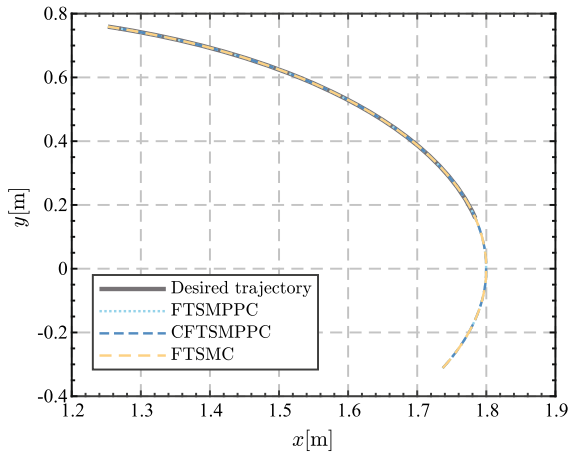

Fig. 5 Tracking trajectories of the robotic manipulator in the workspace

6 kg · m^2. The time-varying external disturbances are set as $\boldsymbol{\tau_d} = [2\sin(t) + 0.5\sin(200\pi t), \cos(2t) + 0.5\sin(200\pi t)]^T$, and the reference trajectories are set as $\boldsymbol{q_d} = \left[1.25 - \frac{7}{5}\exp(-t) + \frac{7}{20}\exp(-4t), 1.25 + \exp(-t) - \frac{1}{4}\exp(-4t)\right]^T$ (rad). The initial states of the joints are given as $q_1(0) = -0.4, q_2(0) = 2.5, \dot{q}_1(0) = \dot{q}_2(0) = 0$.

To illustrate the advantages of the proposed controller, the fixed-time sliding mode control (FTSMC) in [23] is used as a comparator. Furthermore, the proposed PPF is applied to FTSMC in [23], denoted as FTSMPPC, to illustrate the effectiveness of our proposed PPF. For a fair comparison, the control parameters of CFTSMPPC and FTSMPPC are set the same. The parameters of the controllers are chosen in Table 1.

The simulation results are shown in Figs. 3, 4 and 5. As shown in Fig. 3, all three control schemes complete the tracking task. With the proposed PPF, the proposed controller and FTSMPPC have higher tracking accuracy, and the tracking error can remain within the preset PPB. It can be seen that the proposed CFTSMC has a faster convergence rate when the tracking error converges to zero, as described in Remark 4. Meanwhile, from Fig. 4, there are two significant mutations in the control torque of FTSMC and FTSMPPC, which are caused by the discontinuity of the controllers. The proposed controller eliminates the transient change of the control torque by the proposed function $s^p(x)$, as stated in Remark 3. Further, we show the tracking trajectories of the robotic manipulator in the workspace in Fig. 5, where the end of the robotic manipulator can quickly track the desired trajectory by the proposed controller.

Table 1 Simulation parameters of the CFTSMPPC, FTSMPPC and FTSMC

Controller	Parameters
CFTSMPPC/ FTSMPPC	$\boldsymbol{\rho}_0 = [0.8; 0.6]$, $\boldsymbol{\rho}_\infty = [0.002; 0.002]$, $\boldsymbol{\sigma} = [2.01; 2.01]$, $\boldsymbol{\theta} = [0.2; 0.2]$, $\boldsymbol{T} = [5; 6]$, $\delta = 0.01, q = 1.2, p = 0.5, r = 1.2, m_1 = 0.09, \ m_2 = 0.2, k = 1, s_0 = 0.05, b_0 = 12, b_1 = 2.2, b_2 = 2.8, \boldsymbol{K}_0 = 0.1\boldsymbol{I}_2, \boldsymbol{K}_1 = 0.2\boldsymbol{I}_2, \boldsymbol{K}_2 = 0.6\boldsymbol{I}_2$
FTSMC [23]	$\delta = 0.01, q = 1.2, p = 0.5, r = 1.2, m_1 = 0.09, m_2 = 0.2, k = 1, b_0 = 12, b_2 = 2.8, \boldsymbol{K}_0 = \boldsymbol{I}_2, \boldsymbol{K}_1 = 1.5\boldsymbol{I}_2, \boldsymbol{K}_2 = \boldsymbol{I}_2$

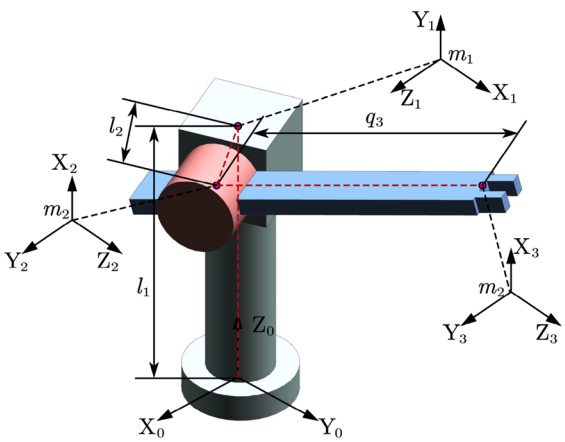

Fig. 6 Architecture of the 3-DOF robotic manipulator

Example 4.2 In this example, a 3-DOF robotic manipulator shown in Fig. 6 is utilized, and its dynamic model has been given in [46]. The 3-DOF robotic manipulator has two rotary joints and a prismatic joint, and the two rotation angles of rotary joints are defined as q_1 and q_2, and the translational of the prismatic joint is defined as q_3. Model parameters of the manipulator are chosen as $l_1 = 0.3$ m, $l_2 = 0.4$ m, $m_1 = m_2 = 2$ kg, $m_3 = 1$ kg. The initial states are set as $q_1 = q_3 = 0.5, q_2 = 1.2, \dot{q}_1(0) = \dot{q}_2(0) = \dot{q}_3(0) = 0$, and the reference trajectories are given as $\boldsymbol{q_d} = \left[\sin\left(\frac{\pi}{5}t\right), 1.5\cos\left(\frac{\pi}{5}t\right), 1 + 0.5\sin\left(\frac{\pi}{5}t\right)\right]^T$. Considering the bounded time-varying disturbance as $\boldsymbol{\tau_d} = [\sin(t) + 1, 2\cos(t) + 0.5, 2\sin(t) + 1]^T$.

To demonstrate the advantages of the proposed controller, three control schemes proposed in recent years include the NFTSMC [7], adaptive nonsingular fast terminal sliding mode control (ANFTSMC) [10], and singularity-free fixed-time sliding mode control (SFSMC) [24] are considered. The NFTSMC and the ANFTSMC are finite-time stable, and the SFSMC scheme is fixed-time stable. All control parameters are chosen in Table 2 and set according to the values given in the references.

It can be seen from Fig. 7 that the proposed control scheme can ensure that the tracking error is always within the preset PPB range. From Fig. 7b, the convergence accuracy of the steady-state error satisfies $|e_i| < 8 \times 10^{-11}$ even with time-varying external disturbances. Figure 8 shows the position tracking error of the joints, and the proposed control scheme has a significantly higher accuracy control performance and a faster transient response over the other control schemes. Although the SFSMC can also guarantee the fixed-time stability, it has the lowest position tracking accuracy. Furthermore, for the velocity tracking error of the robotic manipulator in Fig. 9, the proposed control scheme also shows a significantly higher tracking accuracy. Figure 10 shows the control torques of several control schemes, and we can obtain that the proposed control scheme has a smooth and continuous torque, and the control torque range is much smaller than those of the other control schemes. Figure 11 shows the tracking trajectory of the end of the robotic manipulator in the workspace. The two described finite-time controllers have slower convergence rates, consistent with the results shown in Fig. 8.

5 Comparative study and discussion

To quantitatively evaluate the performance of the control schemes in Example 2, we first present the actual convergence time t_s, Steady-state error e_ρ, maximum control torque $\tau_{\max}$, and the simulation results are shown in Table 3. Considering external disturbances, the proposed control scheme has significant advantages over the existing control schemes regarding convergence rate, tracking error, and the maximum control torque. It is worth mentioning that although actuator saturation is not considered in the simulation, in the

Table 2 Simulation parameters of the CFTSMPPC, NFTSMC, ANFTSMC and SFSMC

Controller	Parameters
CFTSMPPC	$\boldsymbol{\rho}_0 = 1.2\boldsymbol{I}_{3\times1}, \boldsymbol{\rho}_\infty = 0.002\boldsymbol{I}_{3\times1}, \boldsymbol{\sigma} = 2.01\boldsymbol{I}_{3\times1}, \boldsymbol{\theta} = 0.2\boldsymbol{I}_{3\times1}, \ \boldsymbol{T} = [5; 6; 7], \delta = 0.01, q = 1.2, p = 0.5, r = 1.2, m_1 = 0.9, \ m_2 = 1.1, k = 1, s_0 = 0.05, b_0 = 12, b_1 = 2.2, b_2 = 2.8, \boldsymbol{K}_0 = 0.1\boldsymbol{I}_3, \boldsymbol{K}_1 = 0.2\boldsymbol{I}_3, \boldsymbol{K}_2 = 0.6\boldsymbol{I}_3$
NFTSMC [7]	$\boldsymbol{\Gamma}_1 = \text{diag}\{2, 2, 2\}, \boldsymbol{\Gamma}_2 = \text{diag}\{5/3, 5/3, 5/3\}, M_1 = M_2 = 2, b_0 = 12, b_1 = 2.2, b_2 = 2.8$
ANFTSMC [10]	$\alpha = 0.2, \beta = 5/3, \eta = 0.5, k = 250, \lambda_0 = \lambda_1 = \lambda_2 = 0.01, k_1 = k_2 = 1, \hat{b}_0(0) = \hat{b}_1(0) = \hat{b}_2(0) = 0$
SFSMC [24]	$\delta = 0.3, \alpha = 0.7, r = 1.7, \beta = 1.9, \boldsymbol{C}_1 = \boldsymbol{C}_2 = 2\boldsymbol{I}_3, \boldsymbol{K}_1 = \boldsymbol{K}_2 = 5\boldsymbol{I}_3, \upsilon_1 = 2.5, \upsilon_2 = 0.5, a_0 = 12, a_1 = 2.2, m_1 = 0.9, m_2 = 1.1, k = 1$

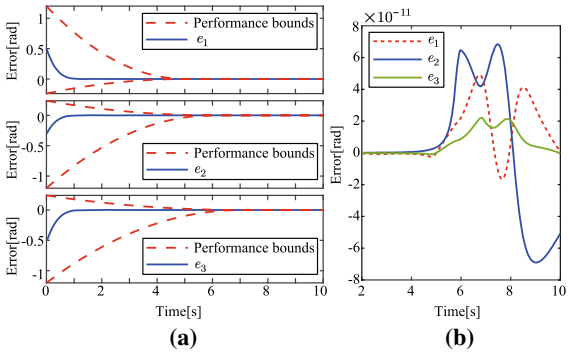

Fig. 7 Position tracking errors of the proposed control scheme. (a) Position tracking error with PPB. (b) Position tracking error in the given range

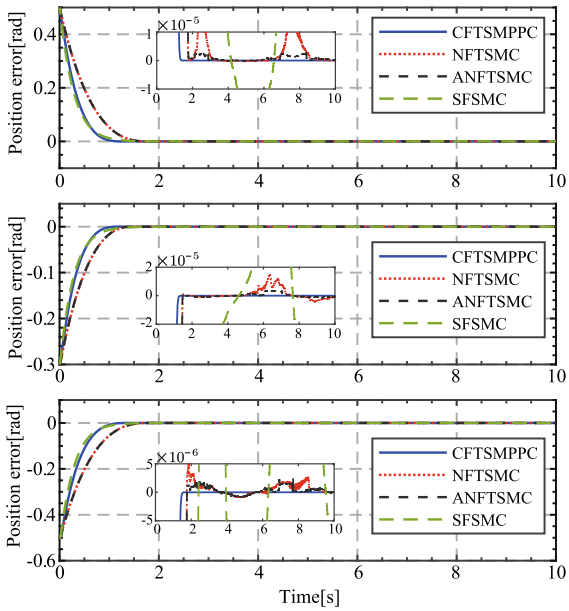

Fig. 8 Position tracking errors with different control schemes

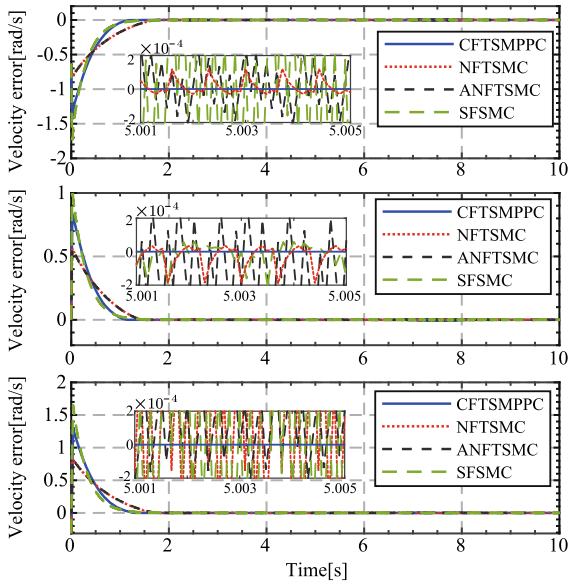

Fig. 9 Velocity tracking errors with different control schemes

actual control, the actuator may not be able to provide a large control torque due to physical constraints. Compared to other control schemes [7,10,24], the proposed control scheme has a smaller control torque range that contributes to its practical application.

Further, we introduce the definition of the following three metrics to evaluate the control performance of the above four control schemes, including the integrated absolute error (IAE), the energy of control input (ECI), and the absolute input chattering error (AICE) [25], and they can be represented as:

$$|e_i|_{\text{IAE}} = \sum_{k=1}^{N} |e_i\,(k)\,| \tag{80}$$

Table 3 The performance of the control schemes in Example 2

controller	Joint 1			Joint 2			Joint 3			PPC	Fixed-time
	t_s(s)	e_ρ(rad)	$\tau_{\max}$(Nm)	t_s(s)	e_ρ(rad)	$\tau_{\max}$(Nm)	t_s(s)	e_ρ(rad)	$\tau_{\max}$(Nm)		
CFTSMPPC	1.37	4.92×10^{-11}	12.19	1.35	6.90×10^{-11}	14.96	1.53	2.21×10^{-11}	15.17	Yes	Yes
NFTSMC [7]	1.77	1.89×10^{-5}	39.62	1.47	1.52×10^{-5}	203.39	1.75	5.25×10^{-6}	100.52	No	No
ANFTSMC [10]	1.79	2.81×10^{-6}	26.24	1.47	4.21×10^{-6}	20.64	1.76	2.60×10^{-6}	39.44	No	No
SFSMC [24]	2.20	3.08×10^{-4}	23.41	2.12	1.30×10^{-4}	29.04	2.35	1.23×10^{-4}	45.37	No	Yes

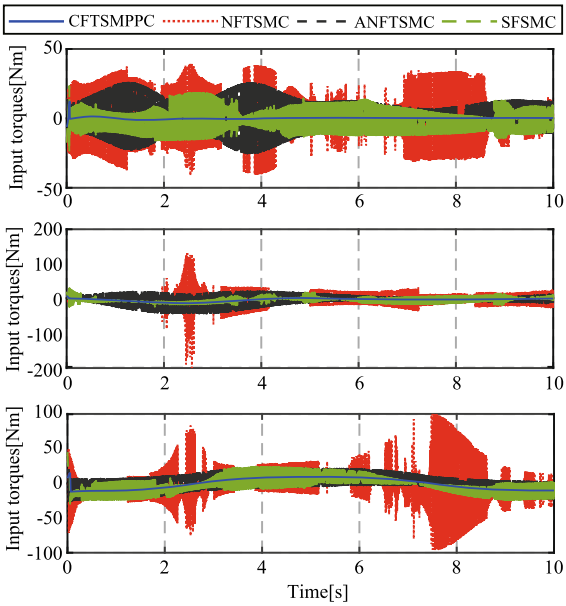

Fig. 10 Control input torques with different control schemes

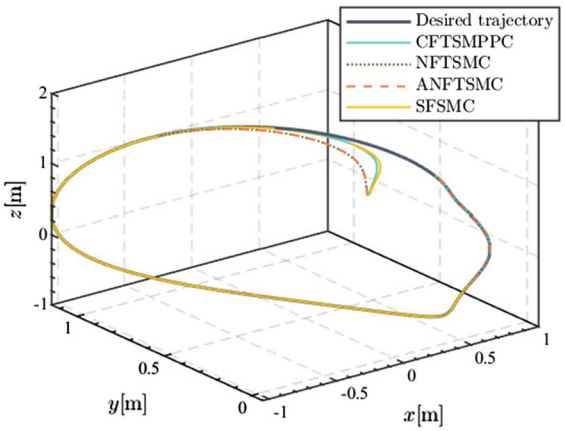

Fig. 11 Tracking trajectories of the robotic manipulator in the workspace

$$|\tau_i|_{\mathrm{ECI}} = \sum_{k=1}^{N} |\tau_i(k)|^2 \tag{81}$$

$$|\Delta\tau_i|_{\mathrm{AICE}} = \sum_{k=1}^{N-1} |\tau_i(k+1) - \tau_i(k)|, \tag{82}$$

where N is the total number of samples, and i denotes the joint number. To avoid the influence of initial error on IAE, only values with time greater than 2 s are considered for $|e_i|$. Meanwhile, for convenience, CFT is used to represent the proposed CFTSMPPC scheme, NFT is the NFTSMC scheme, ANF is the ANFTSMC scheme, and SFS is the SFSMC scheme. As shown in Figs. 12, 13 and 14, the proposed control scheme has smaller IAE, ECI, and AICE than others. It can obtain that the proposed controller has obvious advantages, especially for tracking error and chattering suppression. According to Fig. 12, the proposed scheme only consumes 8.84% energy of the NFTSMC scheme and obtains a better tracking control performance. In conclusion, the proposed control scheme shows the excellent performance in tracking accuracy, energy consumption, and chattering suppression of the robotic system, and is more suitable for practical control of the robotic manipulator than these existing schemes.

The comparison of the above quantitative indicators and the analysis of the two examples in Sect. 4 allow us to highlight the contributions of the proposed control scheme as follows:

1. Compared with the SMC schemes without PPB, the designed PPF contributes to improving the tracking accuracy of the robotic manipulator and making the tracking error converge to the prescribed bounds. Compared with the existing SMC schemes [7,10,23,24], the proposed controller can guarantee the transient performance of the system and improve the control accuracy. It is worth noting that

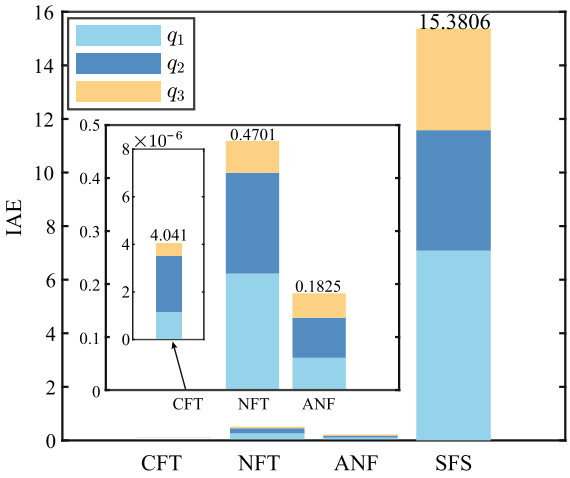

Fig. 12 IAE of different controllers

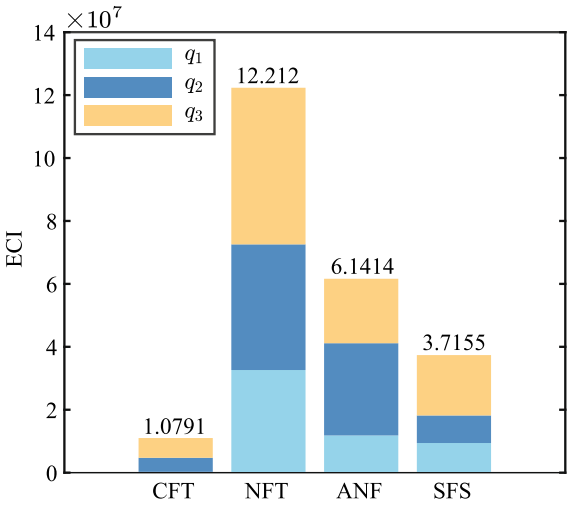

Fig. 13 ECI of different controllers

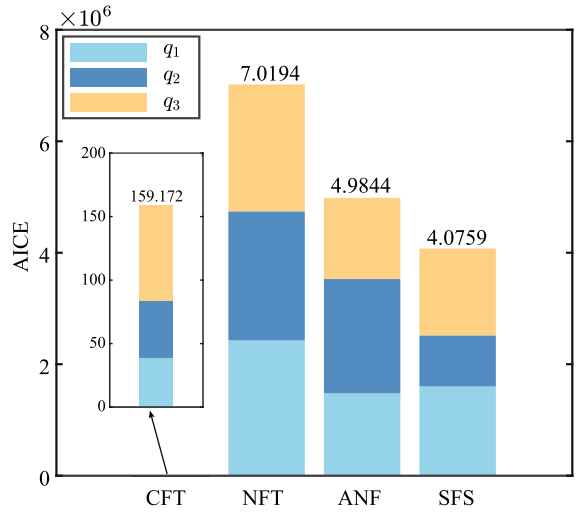

Fig. 14 AICE of different controllers

the proposed PPF is a generic function that can also be applied to other SMC algorithms.

2. Compared with the conventional SMC and the finite-time SMC, the proposed fixed-time SMC scheme is singularity-free and can guarantee that the settling time is independent of the initial states. Benefiting from the proposed sliding surface, the proposed controller can achieve a faster convergence of the tracking error despite requiring more tuning parameters and more complex control techniques compared to conventional SMC. Moreover, with Definition 3, the proposed controller can be considered as predefined-time stable if $T_i \leqslant T_{\max}$, i.e., the tracking error of the system converges to the region R_δ bounded with T_i in (20). Therefore, the upper bound of the settling time can be easily determined by the parameter T_i, thus providing high certainty in the system behavior, which is the most significant advantage of the predefined-time control [47].
3. The chattering-free control torque is a significant advantage of the proposed scheme. Compared to the fixed-time SMC schemes in [23] and [24], the proposed controller ensures smooth control torque without sacrificing the convergence rate even with the coupled uncertainty, benefits to the designed smoothing function $s^p(x)$. Therefore, the proposed control scheme has significant advantages over the existing SMC schemes regarding energy consumption and chattering suppression.

6 Conclusion

In this work, an approximate CFTSMC with prescribed performance is proposed for uncertain robotic manipulators. A fixed-time PPF is designed to ensure the transient and steady-state performance of the position tracking control within fixed time. Meanwhile, a novel CFTSMPPC method is proposed to force the tracking error of the uncertain robotic manipulator to converge to a defined small region in a fixed time which is up bounded by a constant independently of initial states and then converge exponentially to zero. Based on the Lyapunov stability theory, the fixed-time stability of

the proposed controller is rigorously proved. Several numerical simulation results illustrate the effectiveness of the proposed controller in tracking control for robotic manipulators with external disturbances while ensuring high tracking accuracy, low energy consumption, and chattering-free. Some future work is focused on the experimental evaluation of our control scheme through a collaborative robotic manipulator to demonstrate the effectiveness of our proposed control scheme in engineering applications.

Funding This work was supported in part by the National Natural Science Foundation of China (11972343).

Data availability Data sharing is not applicable to this article as no datasets were generated or analyzed during the current study.

Declarations

Conflicts of interest There are no conflicts of interest.

Appendix A: The proof of Lemma 2

Proof For inequality (6), with a positive constant α, we can obtain that

$$\lim_{x\to 0^+}\frac{d|x|^{\alpha+1}}{dx}=\lim_{x\to 0^+}\frac{dx^{\alpha+1}}{dx}=(\alpha+1)\,x^{\alpha}=(\alpha+1)\,|x|^{\alpha}\mathrm{sgn}\,(x) \tag{A1}$$

$$\lim_{x\to 0^-}\frac{d|x|^{\alpha+1}}{dx}=\lim_{x\to 0^-}\frac{d\,(-x)^{\alpha+1}}{dx}=-(\alpha+1)\,(-x)^{\alpha}=-(\alpha+1)\,|x|^{\alpha}=(\alpha+1)\,|x|^{\alpha}\mathrm{sgn}\,(x)\,. \tag{A2}$$

Then, for inequality (7), we have

$$\lim_{x\to 0^+}\frac{d|x|^{\alpha+1}\mathrm{sgn}\,(x)}{dx}=\lim_{x\to 0^+}\frac{dx^{\alpha+1}}{dx}=(\alpha+1)\,x^{\alpha}=(\alpha+1)\,|x|^{\alpha} \tag{A3}$$

$$\lim_{x\to 0^-}\frac{d|x|^{\alpha+1}\mathrm{sgn}\,(x)}{dx}=\lim_{x\to 0^-}\frac{d\left[-(-x)^{\alpha+1}\right]}{dx}=(\alpha+1)\,(-x)^{\alpha}=(\alpha+1)\,|x|^{\alpha}. \tag{A4}$$

Hence, inequalities (6) and (7) hold. □

Appendix B: The proof of Proposition 3

Proof The time derivative of $\rho_i\,(t)$ is

$$\dot{\rho}_i\,(t)=\begin{cases}-\frac{\sigma_i}{T_i}\,(\rho_{0i}-\rho_{\infty i})\left(1-\frac{t}{T_i}\right)^{\sigma_i-1}, & 0\leqslant t<T_i\\ 0, & t\geqslant T_i\end{cases}. \tag{B5}$$

When $0\leqslant t<T_i$, it can be obtained that $\dot{\rho}_i<0$ with $\rho_{0i}>\rho_{\infty i}$. In light of (20) and (B5), it has

$$\lim_{t\to T_i^-}\rho_i\,(t)=(\rho_{0i}-\rho_{\infty i})\left(1-\frac{T_i}{T_i}\right)^{\sigma_i}+\rho_{\infty i}=\rho_{\infty i}=\lim_{t\to T_i^+}\rho_i\,(t) \tag{B6}$$

$$\lim_{t\to T_i^-}\dot{\rho}_i\,(t)=-\frac{\sigma_i}{T_i}\,(\rho_{0i}-\rho_{\infty i})\left(1-\frac{T_i}{T_i}\right)^{\sigma_i-1}=0=\lim_{t\to T_i^+}\dot{\rho}_i\,(t)\,. \tag{B7}$$

Hence, $\rho_i\,(t)$ is monotone decreasing bounded smooth positive function. Due to the fact $\rho_i\,(0)=\rho_{0i}$ and $\rho_i\,(\infty)=\rho_{\infty i}$, we can get $0<\rho_{\infty i}\leqslant\rho_i\,(t)\leqslant\rho_{0i}$. With (B6), we have $\lim_{t\to T_i}\rho_i\,(t)=\rho_{\infty i}$, The proof of Proposition 3. □

Appendix C: The proof of Proposition 4

Proof The derivative of $\psi\,(x)$ with respect to x is

$$\dot{\psi}\,(x)=\frac{-\underline{b}_i\bar{b}_i\exp\,(x)\left(\bar{b}_i-\underline{b}_i\right)}{\left(\underline{b}_i\exp\,(x)-\bar{b}_i\right)^2}. \tag{C8}$$

It is easy to have $\psi\,(0)=0$. According to $\underline{b}_i<0<\bar{b}_i$, we have $\dot{\psi}\,(x)>0$, hence $\psi\,(x)$ is a monotonically increasing function. It has $\lim_{x\to\infty}\psi\,(x)=\frac{\underline{b}_i\bar{b}_i(\exp(\infty)-1)}{\underline{b}_i\exp(\infty)-\bar{b}_i}=\bar{b}_i$ and $\lim_{x\to-\infty}\psi\,(x)=\frac{\underline{b}_i\bar{b}_i(\exp(-\infty)-1)}{\underline{b}_i\exp(-\infty)-\bar{b}_i}=\underline{b}_i$, so we can have $\psi\,(x)\in\left(\underline{b}_i,\bar{b}_i\right)$. According to (12), it can obtain $e_i\in\left(\underline{b}_i\rho_i\,(t),\bar{b}_i\rho_i\,(t)\right)$, so Proposition 4 has been proved. □

Appendix D: The proof of Proposition 5

Proof From Proposition 3, we have $\rho_i > 0$ and $\dot{\rho}_i \leqslant 0$. Considering α_i defined in (26), it can obtain $\alpha_i \geqslant 0$. From Proposition 4, we can have $\frac{e_i(t)}{\rho_i(t)} - \underline{b}_i > 0$ and $\bar{b}_i - \frac{e_i(t)}{\rho_i(t)} > 0$. According to the triangle inequality $a + b \geqslant 2\sqrt{ab}$ with $a \geqslant 0$ and $b \geqslant 0$, it has

$$\begin{aligned}\beta_i &= \left(\frac{1}{e_i/\rho_i - \underline{b}_i} + \frac{1}{\bar{b}_i - e_i/\rho_i}\right)/\rho_i \\ &\geqslant \frac{2}{\rho_i}\sqrt{\frac{1}{\left(e_i/\rho_i - \underline{b}_i\right)\left(\bar{b}_i - e_i/\rho_i\right)}}.\end{aligned} \tag{D9}$$

If and only if $\frac{1}{e_i/\rho_i - \underline{b}_i} = \frac{1}{\bar{b}_i - e_i/\rho_i}$, the equality in (D9) holds, which means that β_i can get the minimum value when $\frac{e_i}{\rho_i} = \frac{\underline{b}_i + \bar{b}_i}{2}$. As a consequence, β_i satisfies

$$\beta_i \geqslant \frac{4}{\rho_i\left(\bar{b}_i - \underline{b}_i\right)}. \tag{D10}$$

From (13), it has $\bar{b}_i - \underline{b}_i < 2$, then we can have $\beta_i > 2\rho_{0i}^{-1}$. Proposition 5 has been proved. □

References

1. Cao, S., Sun, L., Jiang, J., Zuo, Z.: Reinforcement learning-based fixed-time trajectory tracking control for uncertain robotic manipulators with input saturation. IEEE Trans. Neural Netw. Learn. Syst. (2021). https://doi.org/10.1109/TNNLS.2021.3116713
2. Boutalbi, O., Benmahammed, K., Boukezata, B.: An adaptive finite-time stable control law for manipulator robots with unknown parameters. Int. J. Robust Nonlinear Control **31**(11), 5218–5243 (2021)
3. Sai, H., Xu, Z., Li, Y., Wang, K.: Adaptive nonsingular fast terminal sliding mode impedance control for uncertainty robotic manipulators. Int. J. Precis. Eng. Manuf. **22**(12), 1947–1961 (2021)
4. Hong, Y., Xu, Y., Huang, J.: Finite-time control for robot manipulators. Syst. Control Lett. **46**(4), 243–253 (2002)
5. Truong, T.N., Vo, A.T., Kang, H.J.: A backstepping global fast terminal sliding mode control for trajectory tracking control of industrial robotic manipulators. IEEE Access. **9**, 31921–31931 (2021)
6. Feng, Y., Yu, X., Man, Z.: Non-singular terminal sliding mode control of rigid manipulators. Automatica **38**(12), 2159–2167 (2002)
7. Yang, L., Yang, J.: Nonsingular fast terminal sliding-mode control for nonlinear dynamical systems. Int. J. Robust Nonlinear Control **21**(16), 1865–1879 (2011)
8. Slotine, J.J.E., Li, W., et al.: Applied nonlinear control, vol. 199. Prentice hall Englewood Cliffs, NJ (1991)
9. Li, P., Ma, J., Zheng, Z., Geng, L.: Fast nonsingular integral terminal sliding mode control for nonlinear dynamical systems. In: 53rd IEEE conference on decision and control. IEEE; pp. 4739–4746 (2014)
10. Boukattaya, M., Mezghani, N., Damak, T.: Adaptive nonsingular fast terminal sliding-mode control for the tracking problem of uncertain dynamical systems. ISA Trans. **77**, 1–19 (2018)
11. Tao, M., Chen, Q., He, X., Xie, S.: Fixed-time filtered adaptive parameter estimation and attitude control for quadrotor UAVs. IEEE Trans. Aerosp. Electron. Syst. (2022). https://doi.org/10.1109/TAES.2022.3159770
12. Xiao, X., Joshi, S.: Process planning for five-axis support free additive manufacturing. Addit. Manuf. **36**, 101569 (2020)
13. Xiao, X., Roh, B.M., Hamilton, C.: Porosity management and control in powder bed fusion process through process-quality interactions. CIRP J. Manuf. Sci. Technol. **38**, 120–128 (2022)
14. Polyakov, A.: Nonlinear feedback design for fixed-time stabilization of linear control systems. IEEE Trans. Autom. Control **57**(8), 2106–2110 (2011)
15. Zuo, Z., Tie, L.: A new class of finite-time nonlinear consensus protocols for multi-agent systems. Int. J. Control **87**(2), 363–370 (2014)
16. Polyakov, A., Efimov, D., Perruquetti, W.: Finite-time and fixed-time stabilization: implicit Lyapunov function approach. Automatica **51**, 332–340 (2015)
17. Zuo, Z., Tie, L.: Distributed robust finite-time nonlinear consensus protocols for multi-agent systems. Int. J. Syst. Sci. **47**(6), 1366–1375 (2016)
18. Zou, A.M., Kumar, K.D., de Ruiter, A.H.: Fixed-time attitude tracking control for rigid spacecraft. Automatica **113**, 108792 (2020)
19. Liu, Y., Li, H., Zuo, Z., Li, X., Lu, R.: An overview of finite/fixed-time control and its application in engineering systems. IEEE/CAA J. Autom. Sinica. **99**, 1–15 (2022)
20. Zuo, Z.: Nonsingular fixed-time consensus tracking for second-order multi-agent networks. Automatica **54**, 305–309 (2015)
21. Zuo, Z., Han, Q.L., Ning, B., Ge, X., Zhang, X.M.: An overview of recent advances in fixed-time cooperative control of multiagent systems. IEEE Trans. Industr. Inf. **14**(6), 2322–2334 (2018)
22. Jin, X.: Adaptive fixed-time control for MIMO nonlinear systems with asymmetric output constraints using universal barrier functions. IEEE Trans. Autom. Control **64**(7), 3046–3053 (2018)
23. Su, Y., Zheng, C., Mercorelli, P.: Robust approximate fixed-time tracking control for uncertain robot manipulators. Mech. Syst. Signal Process. **135**, 106379 (2020)
24. Zhang, L., Wang, Y., Hou, Y., Li, H.: Fixed-time sliding mode control for uncertain robot manipulators. IEEE Access. **7**, 149750–149763 (2019)
25. Sai, H., Xu, Z., He, S., Zhang, E., Zhu, L.: Adaptive nonsingular fixed-time sliding mode control for uncertain robotic manipulators under actuator saturation. ISA Trans. **123**, 46–60 (2022)

26. Ilchmann, A., Ryan, E.P., Sangwin, C.J.: Tracking with prescribed transient behaviour. ESAIM: Control, Optim. Calc. Var. **7**, 471–493 (2002)
27. Han, S.I., Lee, J.M.: Improved prescribed performance constraint control for a strict feedback non-linear dynamic system. IET Control Theory Appl. **7**(14), 1818–1827 (2013)
28. Bechlioulis, C.P., Rovithakis, G.A.: Robust adaptive control of feedback linearizable MIMO nonlinear systems with prescribed performance. IEEE Trans. Autom. Control **53**(9), 2090–2099 (2008)
29. Guan, Z., Ma, Y., Zheng, Z., Guo, N.: Prescribed performance control for automatic carrier landing with disturbance. Nonlinear Dyn. **94**(2), 1335–1349 (2018)
30. Zhu, C., Zeng, J., Huang, B., Su, Y., Su, Z.: Saturated approximation-free prescribed performance trajectory tracking control for autonomous marine surface vehicle. Ocean Eng. **237**, 109602 (2021)
31. Karayiannidis, Y., Doulgeri, Z.: Model-free robot joint position regulation and tracking with prescribed performance guarantees. Robot. Auton. Syst. **60**(2), 214–226 (2012)
32. Jing, C., Xu, H., Niu, X.: Adaptive sliding mode disturbance rejection control with prescribed performance for robotic manipulators. ISA Trans. **91**, 41–51 (2019)
33. Yang, P., Su, Y.: Proximate fixed-time prescribed performance tracking control of uncertain robot manipulators. IEEE/ASME Trans. Mechatron. (2021). https://doi.org/10.1109/TMECH.2021.3107150
34. Li, X., Luo, X., Wang, J., Guan, X.: Finite-time consensus of nonlinear multi-agent system with prescribed performance. Nonlinear Dyn. **91**(4), 2397–2409 (2018)
35. Zhang, R., Xu, B., Zhao, W.: Finite-time prescribed performance control of MEMS gyroscopes. Nonlinear Dyn. **101**(4), 2223–2234 (2020)
36. Bhat, S.P., Bernstein, D.S.: Finite-time stability of continuous autonomous systems. SIAM J. Control. Optim. **38**(3), 751–766 (2000)
37. Sánchez-Torres, J.D., Gómez-Gutiérrez, D., López, E., Loukianov, A.G.: A class of predefined-time stable dynamical systems. IMA J. Math. Control. Inf. **35**(Supplement-1), i1–i29 (2018)
38. Courant, R., John, F.: Introduction to calculus and analysis I. Springer, Berlin (2012)
39. Spong, M.W., Hutchinson, S., Vidyasagar, M., et al.: Robot modeling and control, vol. 3. Wiley, New York (2006)
40. Zhu, W.H.: Comments on Robust tracking control for rigid robotic manipulators. IEEE Trans. Autom. Control **45**(8), 1577–1580 (2000)
41. Bechlioulis, C.P., Rovithakis, G.A.: Prescribed performance adaptive control for multi-input multi-output affine in the control nonlinear systems. IEEE Trans. Autom. Control **55**(5), 1220–1226 (2010)
42. Bechlioulis, C.P., Rovithakis, G.A.: Robust partial-state feedback prescribed performance control of cascade systems with unknown nonlinearities. IEEE Trans. Autom. Control **56**(9), 2224–2230 (2011)
43. Jing, Y., Liu, Y., Zhou, S.: Prescribed performance finite-time tracking control for uncertain nonlinear systems. J. Syst. Sci. Complex. **32**(3), 803–817 (2019)
44. Zhang, L., Liu, J., Cui, N.: Backstepping control for a two-link manipulator with appointed-time convergence. ISA Trans. (2021). https://doi.org/10.1016/j.isatra.2021.10.005
45. Mondal, S., Mahanta, C.: Adaptive second order terminal sliding mode controller for robotic manipulators. J. Franklin Inst. **351**(4), 2356–2377 (2014)
46. He, W., Huang, H., Ge, S.S.: Adaptive neural network control of a robotic manipulator with time-varying output constraints. IEEE Trans. Cybernet. **47**(10), 3136–3147 (2017)
47. Sánchez-Torres, J.D., Muñoz-Vázquez, A.J., Defoort, M., Aldana-López, R., Gómez-Gutiérrez, D.: Predefined-time integral sliding mode control of second-order systems. Int. J. Syst. Sci. **51**(16), 3425–3435 (2020)